PNAS
www.pnas.org

Supplementary Information for

Starvation sensing by mycobacterial RelA/SpoT homologue through constitutive surveillance of translation

Yunlong Li[1#], Soneya Majumdar[2#], Ryan Treen[1,3#], Manjuli R. Sharma[2], Jamie Corro[1,3], Howard B. Gamper[4], Swati R. Manjari[2], Jerome Prusa[5], Nilesh K. Banavali[2], Christina L. Stallings[5], Ya-Ming Hou[4], Rajendra K. Agrawal[2,3*], Anil K. Ojha[1,3*]

*Corresponding authors:
anil.ojha@health.ny.gov
rajendra.agrawal@health.ny.gov

This PDF file includes:

Supplementary text
Figs. S1 to S11
Tables S1, S2 and S3
References for SI reference citations

Supplemental Text (Materials and Methods)

Bacterial growth medium

Mycobacterium smegmatis (mc^2155) and its variant strains were grown shaking at 200 rpm at 37 °C in Middlebrook 7H9 with ADC enrichment (5% albumin, 2% dextrose, 0.85% sodium chloride and 0.003% catalase) and 0.05% (v/v) Tween80. For ribosome purification, cells from saturated cultures were washed with PBS + 0.05% (v/v) Tween80 for three times and then inoculated at 1:100 dilution in Sauton's medium with either 1 mM $ZnSO_4$ for high-zinc condition or 1 μM zinc-chelator (TPEN, N,N,N',N'-Tetrakis(2-pyridylmethyl)ethylenediamine) for low-zinc condition. 7H10ADC agar plate was used for selection of recombinants and colony growth (*M. smegmatis*). *Escherichia coli* (GC5 or BL21) was grown in LB broth or LB agar at 37 °C. Zeocin (25 μg/mL), kanamycin (20 μg/mL), hygromycin (150 μg/mL for *M. smegmatis* and *E. coli*, carbenicillin (50 μg/mL), and apramycin (5 μg/mL) were used for selection as necessary. For recombinant strain harboring acetamide-inducible promoter, cells were cultured in high- or low -zinc Sauton's medium with 0.2% sodium succinate and induced with 0.2% acetamide.

Construction of recombinant plasmids and strains

A list of plasmids, bacterial strains used in this study is provided in Table S1. A list of oligonucleotides used in this study is provided in Table S2. For construction of Δ*rsh* in *M. smegmatis*, the gene was replaced with a zeocin-resistance marker using a PCR-based modified version of the recombineering strategy as previously described (1). For creating $C_{666}G$, $D_{691}R$ and $C_{692}F$ variants of Rsh, the Rsh ORF with 500 bp of upstream sequence was PCR-amplified and cloned between KpnI and XbaI sites of the integrative vector pMH94 (2), resulting in the recombinant plasmid pYL238. Mutations at the respective sites were introduced using pYL238 as a template by PCR-based mutagenesis using the primer pairs listed in Table S2, resulting in pYL240 ($C_{666}G$), pYL241 ($D_{691}R$) and pYL242 ($C_{692}F$). Mutations were sequence-confirmed and

the plasmids pYL238, pYL240, pYL241 and pYL242 were electroporated into the mc^2155:Δ*rsh* strain of *M. smegmatis*. Cells expressing the mutant variants were cultured in nutrient-rich medium and analyzed for Rsh levels by immunoblotting. The integrative plasmid with anhydrotetracycline(ATc)-inducible CRISPRi-dCas9 system targeting the *clpP1* expression was constructed and donated by Dr. Keith Derbyshire as a part of the Mycobacterium Systems Resources (MSR)(3). The *M. smegmatis* strain (YL9) harboring the plasmid was cultured in high- and low-zinc and ClpP1 depletion was induced by ATc as described previously (2).

Recombinant protein expression and purification

Rsh from *M. smegmatis* (Msmeg_2965) and its variants (Rsh_{C666G}, Rsh_{D691R} and Rsh_{C692F}) with an N-terminal His tag fusion were subcloned in pET21b vector using NdeI and HindIII. The plasmids were introduced into BL21 (DE3) pLysS cells for Rsh expression and purification. Briefly, the cells were grown in LB medium to log phase (OD_{600} of 0.7) at 37 °C, when Rsh expression was induced with 0.5 mM IPTG for 4 hours at 37 °C. Induced cells were harvested (8000 rpm, 20 minutes at 4 °C in Thermo Scientific™ Fiberlite™ F12-6 × 500 Fixed-Angle Rotor) and then resuspended in N-I buffer (50 mM Tris (pH 8.0), 300mM NaCl, 5% glycerol, 10 mM imidazole, 1mM PMSF). The cells were further sonicated (Amplitude 30%, 6 cycles of 10 sec on and 60 sec off for) at 4 °C and the soluble protein in the supernatant was separated from the debris by centrifugation (13000 rpm, 20 minutes, 4 °C in Thermo Scientific™ Fiberlite™ F12-6 × 500 Fixed-Angle Rotor) and incubated with pre-equilibrated Ni-NTA resin for 1 hour at 4 °C. After incubation, Ni-NTA resin was washed three times with N-II buffer [50 mM Tris (pH 8.0), 300mM NaCl, 5% (v/v) glycerol, 30 mM imidazole]. Rsh was then eluted with stepwise increments of imidazole (from 60 mM, to 100mM and to 250 mM) in a buffer containing 50 mM Tris (pH 8.0), 300mM NaCl and 5% (v/v) glycerol. Peak fractions with were pooled and imidazole was removed by dialysis in the buffer containing 50 mM Tris (pH 8.0), 300mM NaCl and 30% (v/v) glycerol. For recombinant IF2

(MSMEG_2628) with N-terminal His_{6x} tag, the full-length codon optimized gene with N-terminal 6x-His-sequnce and NdeI-XhoI sites was synthesized (IDT DNA Inc.) (Table S2). The synthetic fragment was cloned into a pET21a vector. Recombinant protein was expressed in BL21-DE3 (pLysS) and purified on Ni-NTA matrix as detailed for His_6-Rsh above.

Ribosome purification

Rsh bound ribosomes were purified with a few modifications from the previously described protocol (1). *M. smegmatis* cells were grown for the specified time in 500 mL of Sauton's media containing 0.05% Tween 80 and either 1 mM $ZnSO_4$ or 1 μM TPEN. Cells were harvested (8000 rpm for 20 minutes in a Thermo Scientific™ Fiberlite™ F12-6 × 500 Fixed-Angle Rotor) and pulverized 6 times at 15 Hz for 3 minutes in a mixer mill (Retsch MM400). The lysates were mixed with 20 mL of HMA-10 buffer (20 mM HEPES-K pH7.5, 30 mM NH_4Cl, 10 mM $MgCl_2$, 5 mM β-mercaptoethanol) and centrifuged for 30 minutes at 30,000g in Thermo Scientific™ Fiberlite™ F12-8 × 50 Fixed-Angle Rotor. The supernatants were collected in the Beckman PC ultracentrifuge tubes and further centrifuged for 2 hours and 15 minutes at 42800 rpm in a Beckman rotor Type 70Ti. Pellets were soaked in 4 mL of HMA-10 buffer in an ice water bath overnight, and then homogenized for 30 minutes. The homogenized pellets were treated with 3 units/mL Rnase-free Dnase (Ambion) for two hours at 4 °C. The contents were transferred to Beckman PA tubes and centrifuged at 22,000 g for 15 minutes in Thermo Scientific™ Fiberlite™ F12-8 × 50 Fixed-Angle Rotor. The supernatants were collected into Beckman ultracentrifuge PC tubes and centrifuged for 2 hours and 15 minutes at 42,800 rpm in a Beckman rotor Type 70Ti. The pellets were dissolved in 1 mL HMA-10 buffer and centrifuged for 10 minutes at 10,000 g. The supernatants containing the crude ribosomes were collected and quantified by measuring their optical density at 260 nm. The crude ribosome preparations were then layered on top of 37 mL sucrose density gradients (10%-40%) and centrifuged for 16 hours at 24,000 rpm in a Beckman rotor SW 28. The 70S ribosome fractions were collected after fractionating the sucrose

gradient in a 260 nm Brandel gradient analyzer as previously described (4). The pooled 70S ribosome fractions pelleted by ultracentrifugation at 42,800 rpm for 3 hours in a Beckman rotor Type 70Ti were suspended in HMA-10 buffer (20 mM HEPES-K pH7.5, 30 mM NH_4Cl, 10 mM $MgCl_2$, 5 mM β-mercaptoethanol) and quantified by measuring absorbance at 260 nm.

MPY-bound ribosomes and other high-salt washed ribosomes were purified exactly as described previously (1, 2). The steps up to homogenization were same as described above. After homogenization, 4 mL of the homogenized suspension was treated with 3 units/mL Rnase-free Dnase (Ambion) for one hour at 4 °C, then 4 mL of HMA-0.06 buffer (20 mM HEPES-K pH 7.5, 600 mM NH_4Cl, 10 mM $MgCl_2$, 5 mM β-mercaptoethanol) was added to the suspension, which was further incubated at 4 °C for 2 hours. The content was transferred to Beckman PA tubes and centrifuged at 22,000 g for 15 minutes in Thermo Scientific™ Fiberlite™ F12-8 × 50 Fixed-Angle Rotor. Supernatants were collected and layered on top of 8 mL 32% sucrose solution in HMA-10 buffer and centrifuged for 16 hours at 37000 rpm in a Beckman rotor Type 70Ti. The supernatant was discarded, and the pellet was rinsed with HMA-10 buffer to remove the brownish material. The crude ribosome was resuspended in 1 mL HMA-10 buffer and centrifuged for 10 minutes at 10,000 g. Supernatant containing the crude ribosome was collected and quantified by measuring optical density at 260nm. 70S ribosome from the crude ribosome was further separated on a 10-40% sucrose density gradient and fractionated as indicated above.

In vitro reconstitution of Rsh with 70S initiation complex

Co-sedimentation of Rsh with the ribosomal subunits: 70S ribosomes were purified from low-zinc culture of isogenic Δ*rsh*/Δ*mpy*/Δ*mrf* triple mutant of *M. smegmatis*. Subunits were dissociated from the purified 70S ribosomes by incubation at 37°C for thirty minutes in HMA-1 buffer (20 mM HEPES-K pH7.5, 30 mM NH_4Cl, 1 mM $MgCl_2$, 5 mM β-mercaptoethanol. The resulting subunits

were then purified from a 10-40% sucrose density gradient. Individual subunits equivalent to A_{260} of 0.3 (7.2 pmol) were mixed with 1.8 pmol of purified recombinant Rsh in 100 μL binding buffer (20 mM HEPES-K pH7.5, 100 mM NH4Cl, 10 mM $MgCl_2$, 5 mM β-mercaptoethanol, 50mM KCl), and the mixture was incubated for thirty minutes at 37°C. The reactions were then layered on 100 μL of 32% sucrose cushion and centrifuged at 42,800 rpm for 3 hours in a Beckman TLA 100 rotor using the Optima-Max TL ultracentrifuge (Beckman Coulter). After centrifugation, the supernatant was discarded, and the ribosome pellet was resuspended in 20 μL HMA-10 buffer. The abundance of Rsh was further determined by immunoblotting using the protocol described below Rsh, and S13, and L33.

Preparation of fMet-tRNA$_i^{Met}$: An *E. coli* culture containing a plasmid borne expression vector for $tRNA_i^{Met}$ under control of the LacI repressor was grown to an optical density at 600 nm of 0.4-0.6 at which time IPTG was added to induce expression of the tRNA. After 8 h the cells were harvested, lysed by phenol, and total tRNA isolated using a series of differential precipitation steps (5). Approximately half of the recovered tRNA was a substrate for charging by MetRS. The charging reaction (2 mL) contained approximately 200 nmoles of total tRNA and 10 nmoles of MetRS in the presence of 1 mM methionine, 2 mM ATP, 10 mM $MgCl_2$, 20 mM KCl, 4 mM DTT, 50 μg/mL BSA, and 50 mM Tris-HCl pH 7.5. After 10 min at 37 °C a 4.0 μL aliquot of the reaction was removed for determination of the charging efficiency as described by Gamper et *al* (6). The remaining reaction was incubated for 10 min at 37 °C with 1.7 μmoles of 10-formyltetrahydrofolate and 20 nmoles of methionyl formyl transferase to convert Met-$tRNA_i^{Met}$ to fMet-$tRNA_i^{Met}$. The reaction was quenched by adding a 0.1 volume of 2.5 M NaOAc pH 5.0. Following an equal volume pH 5 phenol-chloroform-isoamyl alcohol extraction (80:17:3), the tRNA was ethanol precipitated, dissolved in 300 μL 25 mM NaOAc pH 5.0, and stored at -70 °C. Approximately 200 nmoles of tRNA was recovered, of which 45% was fMet-$tRNA_i^{Met}$.

Reconstitution of Rsh-bound 70S initiation complex: 70S ribosomes prepared from a low-zinc culture of isogenic Δ*rsh*/Δ*mpy*/Δ*mrf* triple mutant of *M. smegmatis* were dialyzed at 4°C with low-magnesium buffer (20 mM HEPES-K pH7.5, 30 mM NH_4Cl, 0.5 mM $MgCl_2$, 5 mM β-mercaptoethanol) to dissociate the 30S and 50S subunits. Two rounds of dialysis were performed, with fresh buffer change every four hours. Subunit dissociation was confirmed by loading 2.4 picomoles of the dialyzed ribosomes onto a 10-40% sucrose density gradient. Another 2.4 pmoles of dissociated ribosomes were mixed with five-fold molar excess of fMet-$tRNA_i^{fMet}$, a synthetic mRNA template (GGCAAGGAGGUAAAAAUGUUCAAAAAA-Flour) (IDT, USA), recombinant His_6-IF2, recombinant His_6-Rsh, and either GTP or GMP-PNP (Sigma-Aldrich) in a 100 µL reaction in buffer I (20 mM HEPES-K pH 7.5, 30 mM NH_4Cl, 1 mM $MgCl_2$, 5 mM β-mercaptoethanol), and the mixture was incubated at 37 °C for 15 minutes to allow formation of the initiation complex on the 30S subunit. Then 25 µL of buffer II (20 mM HEPES-K pH7.5, 30 mM NH4Cl, 50 mM MgCl2, 5 mM β-mercaptoethanol, 600mM KCl) was added to the mixture, thereby bringing the final concentration of $MgCl_2$ and KCl to 10mM and 120 mM, respectively. The reaction was then incubated for an additional 30 minutes at 37°C to allow joining of the 50S subunit. Resulting complexes were either used for structural analysis or resolved on a 15 mL 10-40% sucrose density gradient centrifuged at 35000 rpm for 135 minutes using SW41 rotor on an Optima L-90K ultracentrifuge (Beckman Coulter), and the resolved particles were fractionated as previously described (4). For immunoblotting analysis, content of the indicated fractions were precipitated using Methanol-chloroform extraction as previously described (2). Briefly, each fraction was vortexed with 4X volume of methanol for 5-10 seconds and centrifuged for 10 seconds at 13,200 rpm on a benchtop centrifuge before adding one volume of chloroform. The mixture was further centrifuged at 13,200 rpm for 60 seconds, after which 3X volume of water was added and the mixture was vortexed before further centrifugation at 13,200 rpm for 60 seconds. The upper aqueous layer was discarded while retaining the interface and the organic layer, which was mixed with 3X volume of methanol, vortexed and

centrifuged at 13,200 rpm for 2 minutes. The supernatant was discarded, and the resulting pellet was dried and resuspended in 0.1 M Tris containing 8M urea for further analysis of proteins by immunoblotting.

Immunoblotting

Total cell lysates (10 µg) or purified 70S ribosomes (2.4 pmoles) were used for detecting S13, MPY, Mrf-FLAG, and $S14_{C-}$, while 24 pmoles ribosome were used for detecting Rsh. Samples were resolved on 8% SDS-PAGE (for FLAG, Rsh and GroEL analysis) or 12% SDS-PAGE (for MPY, $S14_{C-}$ and S13), and proteins were probed with anti-FLAG (1:5000, Genescript), anti-GroEL (1:5000, Enzo), anti-Rsh of *M. tuberculosis* (1:5000), anti-S13 of *E. coli* (1:100, The Developmental Studies Hybridoma Bank), endogenously raised anti-MPY (1:5000) and anti-$S14_{C-}$ (1:2000) antibodies.

ppGpp extraction and analysis

Cells of specified *M. smegmatis* strains were grown in Sauton's medium with either 1 mM Zn or 1 µM TPEN for 96 hours, after which 1 mL of the culture was labelled with 100 µCi/mL of ^{32}P KH_2PO_4 (Perkin Elmer, 900-1100mCi/mmol) for 6 hours on a shaker at 37 ^{o}C. Labeled cells were washed once with TBST (20mM Tris pH7.6 + 150 mM NaCl + 0.05% Tween 80). Half of the cells (0.5 mL) were pelleted and resuspended in 25 µL of 4M formic acid and kept frozen at -20 ^{o}C until ready for extraction. Remaining 0.5 mL cells were starved for 3 hours in TBST, or metal-chelated TBST, or zinc-supplemented TBST as specified. Following treatment, both pre- and post-starved cells were pelleted and resuspended in 25 µL of 4M formic acid and incubated on ice for 10 minutes. Cell suspensions were frozen on dry ice for 10 minutes and thawed at 37 ^{o}C for 10 minutes. The freeze-thaw cycle was repeated 5 times, after which the cell lysates were centrifuged at 13,500 rpm for 5 minutes at 4 ^{o}C, and 5 µL of the supernatants containing ^{32}P

labeled intracellular nucleotides were resolved on a 20 x 20 cm plastic PEI cellulose F TLC plate (Millipore) using 1.5 M KH_2PO_4 pH 3.4 as a solvent. When the solvent front reached the top of the plate, the plate was dried and exposed to X-ray film. 5 µL of 100 mM nonradioactive nucleotides [ppGpp (Trilink), ATP, GDP and GTP (Thermo Fisher)] were also resolved as positional markers, which were visualized by handheld UV lamp (Stuart, Cole Palmer). For quantitative analysis, pixel density of ppGpp spot were determined from densitometric scan of radiographs using Fiji (ImageJ). Using the counts from low-zinc culture of wild-type strain in a radiograph as the common denominator, relative counts in other samples from the same radiograph were calculated.

Cryo-electron microscopy and image processing

Quantifoil holey carbon copper grids R 1.2/1.3 were coated with a continuous layer of carbon (~50 Å thick). After glow discharge for 30 s on a plasma sterilizer, 4 µL of the 200 nM Rsh-bound 70S initiation complex sample was placed on the grids. The sample was incubated on the grids for 15 s at 4 °C and 100% humidity, followed by blotting for 4 s before flash-freezing into the liquid ethane using a Vitrobot IV (FEI). Data were collected on a Titan Krios electron microscope at 300 keV using a K3 direct electron-detecting camera (Gatan). −1.50 to −2.50 µm defocus range was used at a magnification of 81,000×, yielding a pixel size of 0.846 Å. The dose rate of 23.3 electrons/pixel/second with a 2.05 second exposure time, with 41 frames of 0.05 second duration each, resulted in a total dose of 66.59 e/Å−2. RELION 4.0 (7) was used for data processing. Image stacks were gain-corrected, dose-weighted, and aligned using MotionCor2 (8) for 9,103 micrographs. The contrast transfer function of each aligned micrograph was estimated using CTFFIND-4.1 (9). A subset of micrographs was used for particle picking followed by 2D classification. Relevant 2D classes were used for reference-based particle picking on all micrographs yielding 1,928,609 particles. These particles were 2D classified and class-averages with obvious subunits (50S/30S) and noise were excluded

and only crisp monosome classes with 389,456 particles were selected (Fig. S7). The selected particles were 3D refined and followed by 3D classification. Classes corresponding to monosomes with 349,437 particles were selected for further processing. In order to resolve structural heterogeneity in the monosome particles, we performed 3D refinement using a large subunit mask followed by three rounds of fixed orientation 3D classification. In the first round of fixed orientation 3D classification, we used an SSU mask to resolve the SSU conformations into six classes. Class I with 158,489 particles showed density corresponding to P-site tRNA and Rsh, representing the Rsh-bound 70S initiation complex. We then performed the second round of fixed orientation 3D classification on this class using a mask encompassing the entire inter-ribosomal subunit space such as the L7/L12-stalk, A-, P-, and E-site tRNA binding sites, and the L1-stalk regions. The second round of fixed orientation 3D classification resolved the conformational and particularly compositional heterogeneity in the masked region. We derived four classes with P-site tRNA density and two classes with P-site tRNA and Rsh densities. We performed the third round of fixed orientation 3D classification combining the two classes with P-site tRNA and Rsh densities, (49,058 particles) using a mask encompassing the P-site tRNA and Rsh. Two of the classes, one with 16,013 particle and another with 20,308 particles, showed densities corresponding to P-site tRNA and ZBD and ACT domains of Rsh. However, density corresponding to ACT domain was slightly better in the class with 16,013 particles and was refined to a global resolution of 2.98 Å (Map I) and was used to generate the initial model of the Rsh-ACT domain. Since the densities corresponding to ZBD were very similar in both classes, they were merged. The combined class with a total of 36,321 particles showed significant density corresponding to P-site tRNA and Rsh-ZBD. CTF refinement and Bayesian polishing of the combined class with a total of 36,321 particles yielded a map with a global resolution of 2.7 Å (Map II) and was used to generate the final model of the entire complex including both the Rsh-ZBD and Rsh-ACT domains.

Model building

Coordinates of the large and small subunits from our published C- *M. smegmatis* ribosome structure (PDB:6DZI) were docked as rigid bodies into the cryo-EM map (Map II) using Chimera 1.14 (10). To achieve optimal fitting, we adjusted the model based on the densities in Coot (11). The model was subsequently refined using PHENIX 1.14 (12). A predicted structure of *M. smegmatis* Rsh is available in the Alphafold Protein Structure database (13). This structure was docked into the corresponding density in the cryo-EM map using Chimera 1.14 (10) and subsequently refined with Coot (11) and PHENIX 1.14 (12). A validation report for the model was obtained from PHENIX 1.14 (12). The overall statistics of EM reconstruction and molecular modeling are listed in Table S3. ChimeraX-1.0 (14) and Chimera 1.14 (10) were used to generate the structural figures in the manuscript.

References

1. Y. Li *et al.*, Zinc depletion induces ribosome hibernation in mycobacteria. *Proc Natl Acad Sci U S A* **115**, 8191-8196 (2018).
2. Y. Li, J. H. Corro, C. D. Palmer, A. K. Ojha, Progression from remodeling to hibernation of ribosomes in zinc-starved mycobacteria. *Proc Natl Acad Sci U S A* **117**, 19528-19537 (2020).
3. J. A. Judd *et al.*, A Mycobacterial Systems Resource for the Research Community. *mBio* **12** (2021).
4. Y. Li *et al.*, Purification of Hibernating and Active C- Ribosomes from Zinc-Starved Mycobacteria. *Methods Mol Biol* **2314**, 151-166 (2021).
5. v. Ehrenstein, Isolation of sRNA from intact Escherichia coli cells. *Methods in Enzymology* **12A**, 588-596 (1967).
6. H. Gamper, Y. M. Hou, A Label-Free Assay for Aminoacylation of tRNA. *Genes (Basel)* **11** (2020).
7. S. H. Scheres, RELION: implementation of a Bayesian approach to cryo-EM structure determination. *J Struct Biol* **180**, 519-530 (2012).
8. S. Q. Zheng *et al.*, MotionCor2: anisotropic correction of beam-induced motion for improved cryo-electron microscopy. *Nat Methods* **14**, 331-332 (2017).
9. A. Rohou, N. Grigorieff, CTFFIND4: Fast and accurate defocus estimation from electron micrographs. *J Struct Biol* **192**, 216-221 (2015).
10. E. F. Pettersen *et al.*, UCSF Chimera--a visualization system for exploratory research and analysis. *J Comput Chem* **25**, 1605-1612 (2004).
11. P. Emsley, B. Lohkamp, W. G. Scott, K. Cowtan, Features and development of Coot. *Acta Crystallogr D Biol Crystallogr* **66**, 486-501 (2010).
12. P. D. Adams *et al.*, PHENIX: a comprehensive Python-based system for macromolecular structure solution. *Acta Crystallogr D Biol Crystallogr* **66**, 213-221 (2010).
13. J. Jumper *et al.*, Highly accurate protein structure prediction with AlphaFold. *Nature* **596**, 583-589 (2021).
14. E. F. Pettersen *et al.*, UCSF ChimeraX: Structure visualization for researchers, educators, and developers. *Protein Sci* **30**, 70-82 (2021).

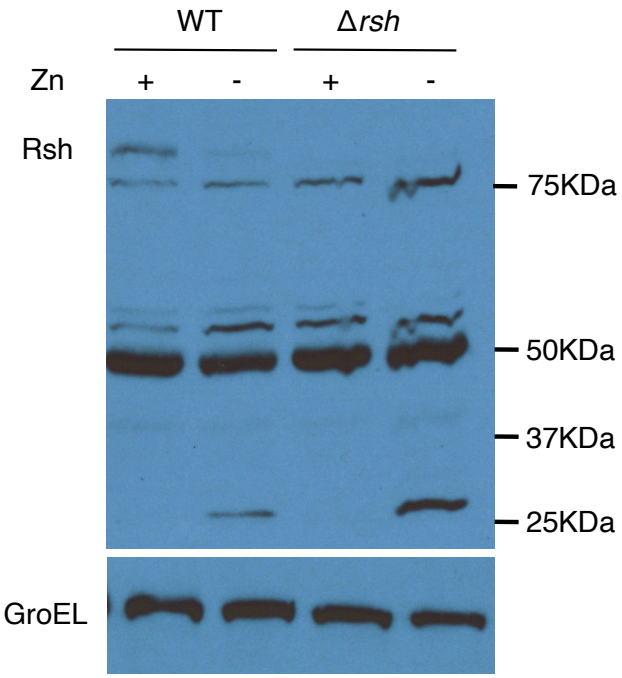

Figure S1: A full-gel immunoblot image of cells lysates from WT and Δ*rsh* strains cultured in high- (1mM $ZnSO_4$; abbreviated as Zn) and low-zinc Sauton's medium (1μM TPEN; abbreviated as T) and probed with anti-Rsh antibody. Data shows lack of any Rsh-derived smaller product in the low-zinc culture. GroEL from the lysate was probed as a loading control.

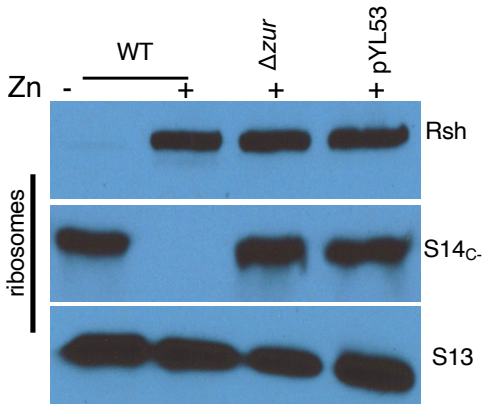

Figure S2: Ribosome remodeling has no effect on Rsh-ribosome interaction. Immunoblot analysis of Rsh bound to 70S ribosomes from 96-hour old high-zinc cultures of WT *M. smegmatis* and its two recombinant strains, Δ*zur* and Δ*c*-:pYL53, which constitutively expressed the remodeled (C-) ribosomes. Low-zinc culture of WT was used as control.

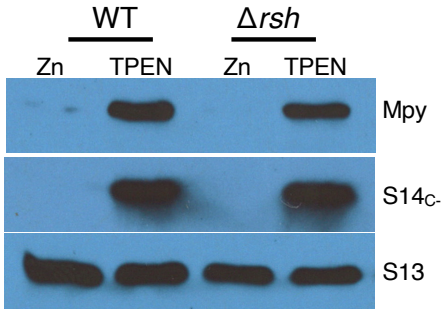

Figure S3: Levels of Mpy in 70S ribosomes purified from high- and low-zinc cultures of WT and Δ*rsh*. $S14_{c-}$ and S13 were probed as controls as indicated.

A

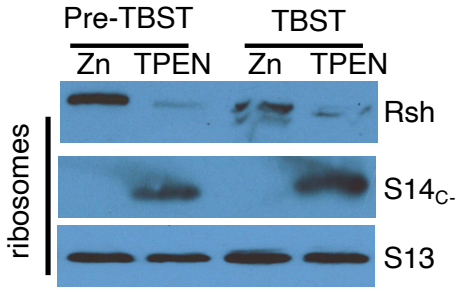

B

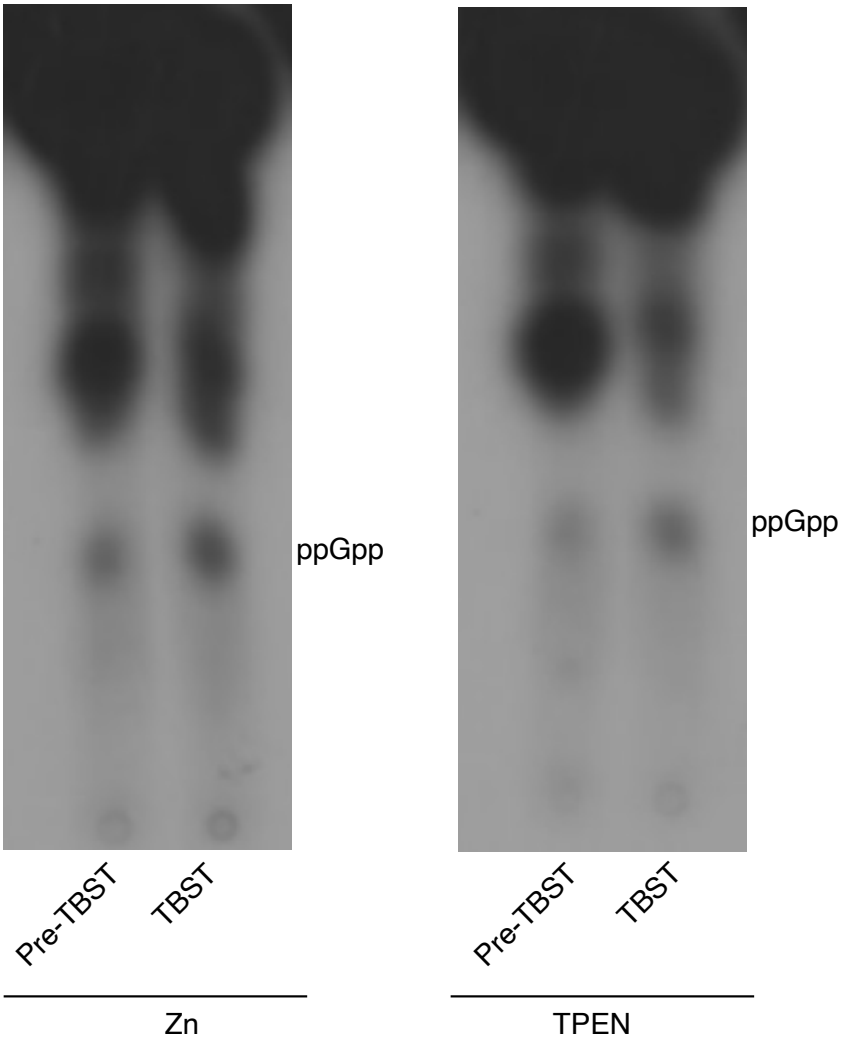

Figure S4: Level of Rsh-bound ribosomes (A) and ppGpp (B) in *M. smegmatis* before and after exposure to starvation (TBST) from high- or low-zinc culture conditions after 28 hours of growth.

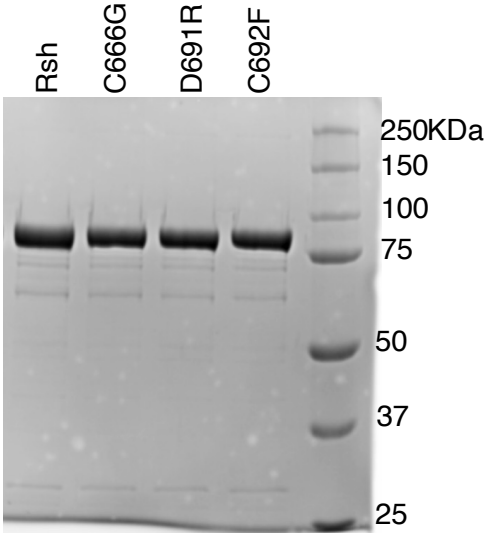

Figure S5: Purified recombinant 6xHis-tagged Rsh proteins expressed from an IPTG-inducible T7 promoter in the *E. coli* BL21 strain and visualized by SDS-PAGE and the Coomassie Blue stain. Each recombinant protein was purified from the same volume of starting cells using the same method, and equal volume of each sample was loaded on the gel.

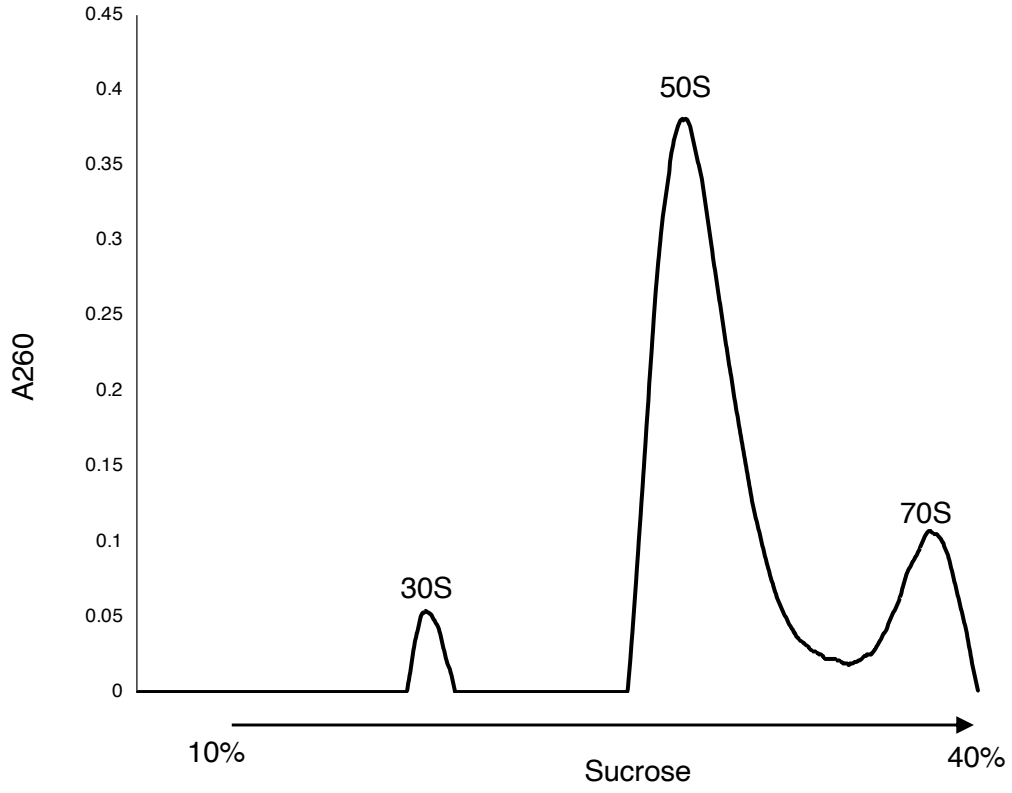

Figure S6: Sucrose density gradient profile of dissociated ribosomes used in the reconstitution experiments described in figures 4B and C. The reconstituted ribosome complex in figure 4C was used for structural studies.

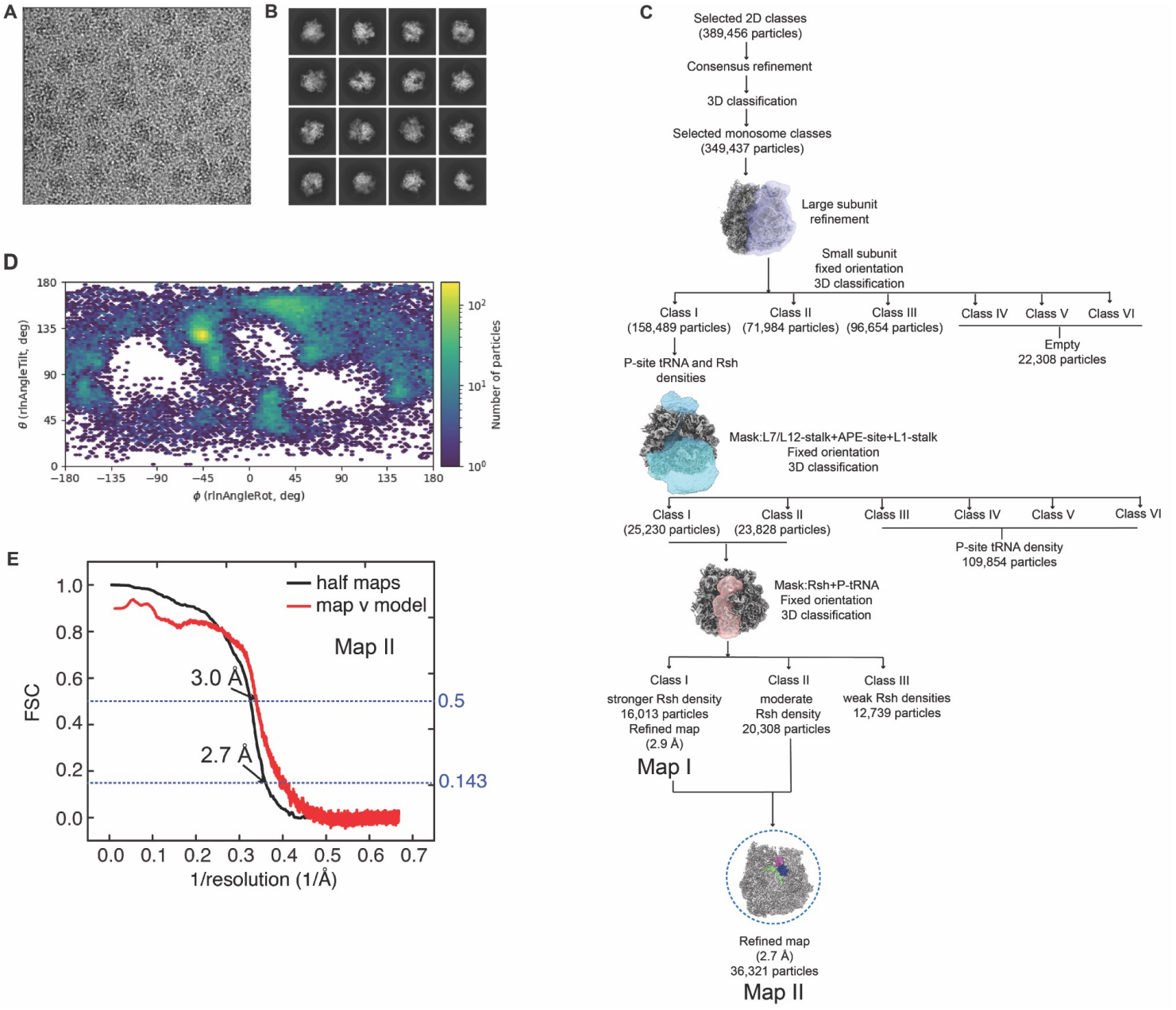

Figure S7: Image processing of *M. smegmatis* 70S-Rsh-fMet-tRNAiMet complex. A. representative micrograph from the *M. smegmatis* 70S-Rsh-fMet-tRNA$_i^{Met}$ complex dataset. **B.** Representative 2D class averages used for the 3D reconstructions. **C.** Flowchart showing the details of 3D classifications and refinements. The 3D map used for model building and functional interpretation is encircled in blue dashes. **D.** The Euler angle heat map for 36,321 particles comprising Map II. E. Gold-standard FSC of Map II (black) overlaid with the map-to-model FSC (red).

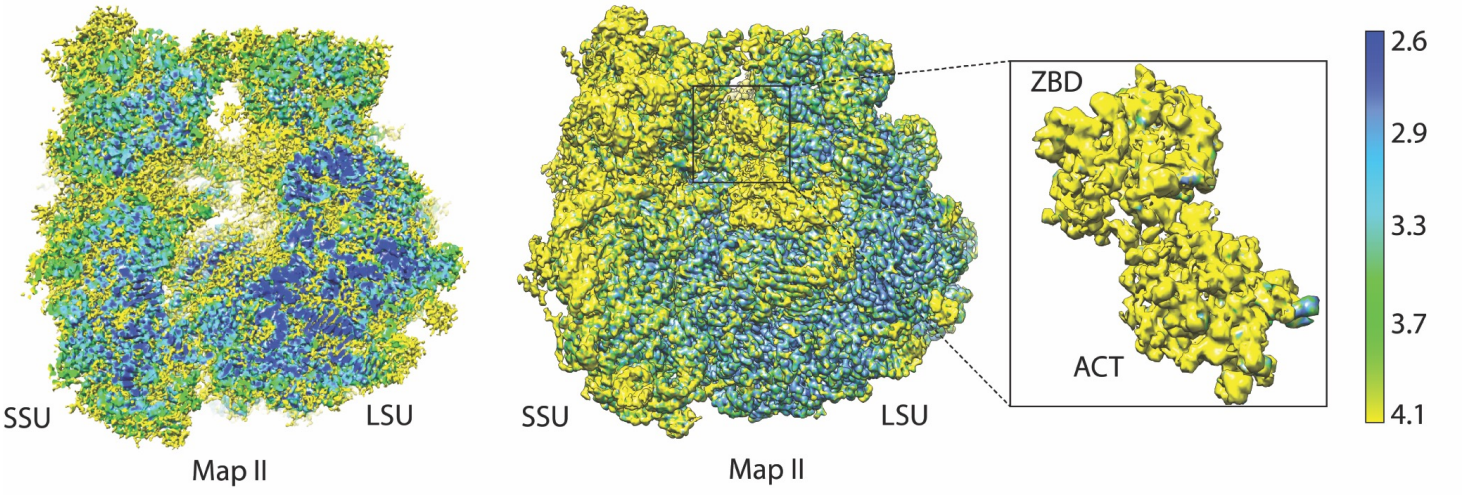

Figure S8: Local resolution of the cryo-EM map (Map II) of *M. smegmatis* 70S-fMet-tRNA$_i^{Met}$-Rsh Complex. A cutting plane has been applied to show the core of the ribosome (left), and the same map without a cutting plane to include the Rsh density and its binding site (right). The inset displays local resolution of the two Rsh domains, ZBD and ACT.

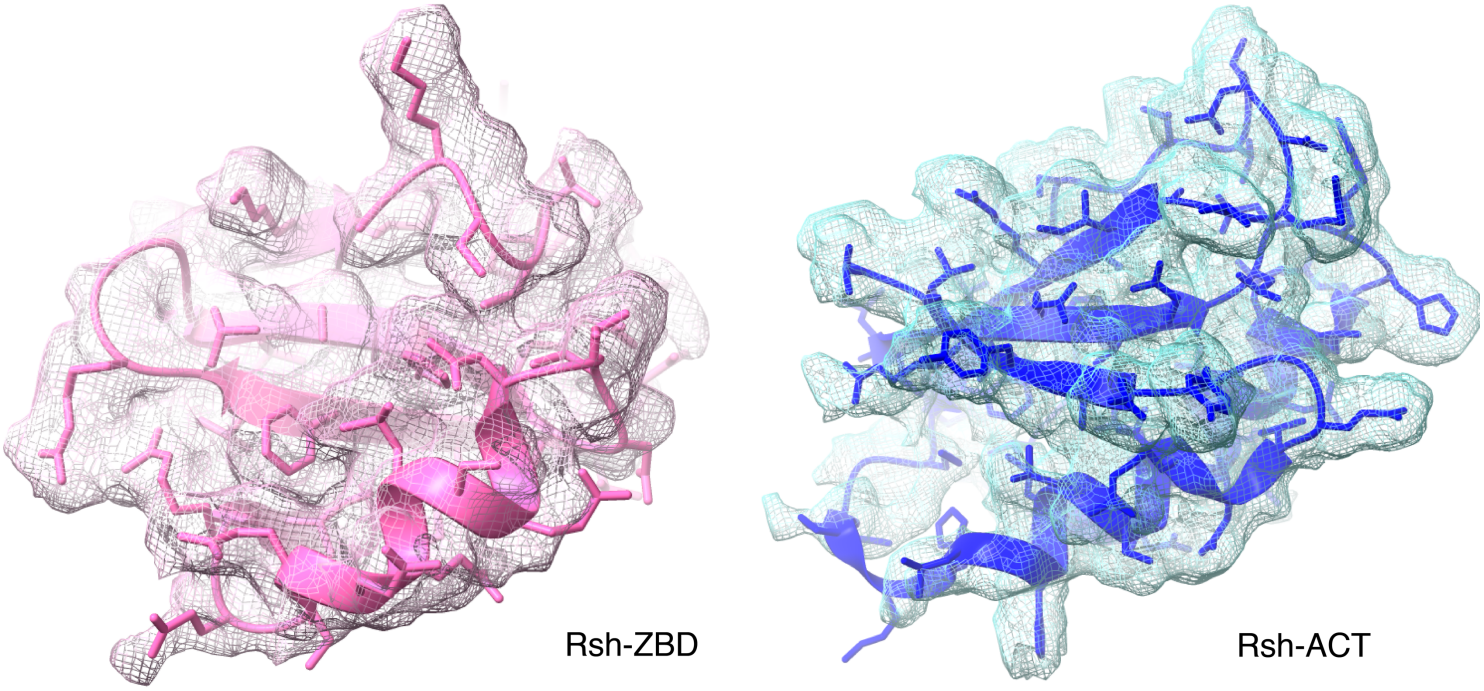

Figure S9: Modeling of the ZB- and ACT domains into corresponding cryo-EM densities. Two different density threshold values were used for modeling the two domains, as density for the main anchoring ZBD (pink) was stronger than that for the ACT domain.

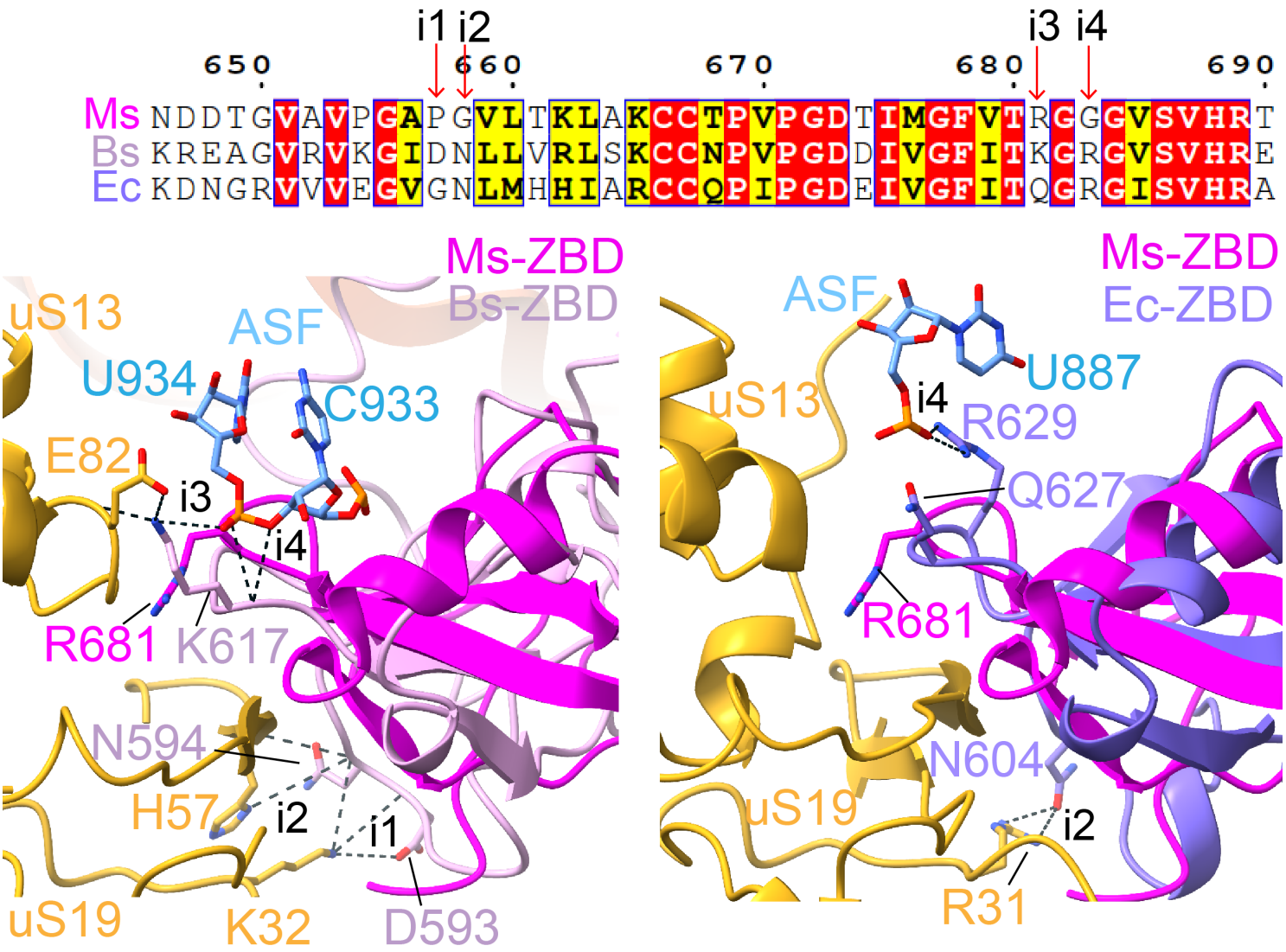

Figure S10: Species-specific differences in Rsh/RelA-ZBD interaction with uS19, uS13, and ASF. Top- Multiple sequence alignment of a short stretch in the ZBD domain of *M. smegmatis* (Ms) Rsh, *B. subtilis* (Bs) Rsh, and *E. coli* (Ec) RelA. Amino acid substitutions at four regions (indicated by red arrows) that result in species-specific differences in interactions (i1-i4) of the ZBD domain with ribosomal components. Bottom left- Superimposition of Ms 70S-Rsh (ZBD, magenta) and Bs 70S-Rsh (ZBD, light pink). Interactions of Bs-Rsh-ZBD with the ribosome that are absent in the case of Ms-Rsh-ZBD are displayed: two with uS19 (i1 and i2), one with uS13 (i3), and one with ASF (i4). Bottom right- Superimposition of Ms 70S-Rsh (ZBD, magenta) and Ec 70S-RelA (ZBD, light purple). Ec RelA-ZBD has two extra interactions with the ribosome, as compared to Ms Rsh-ZBD: One with uS19 (i2) and another with ASF (i4).

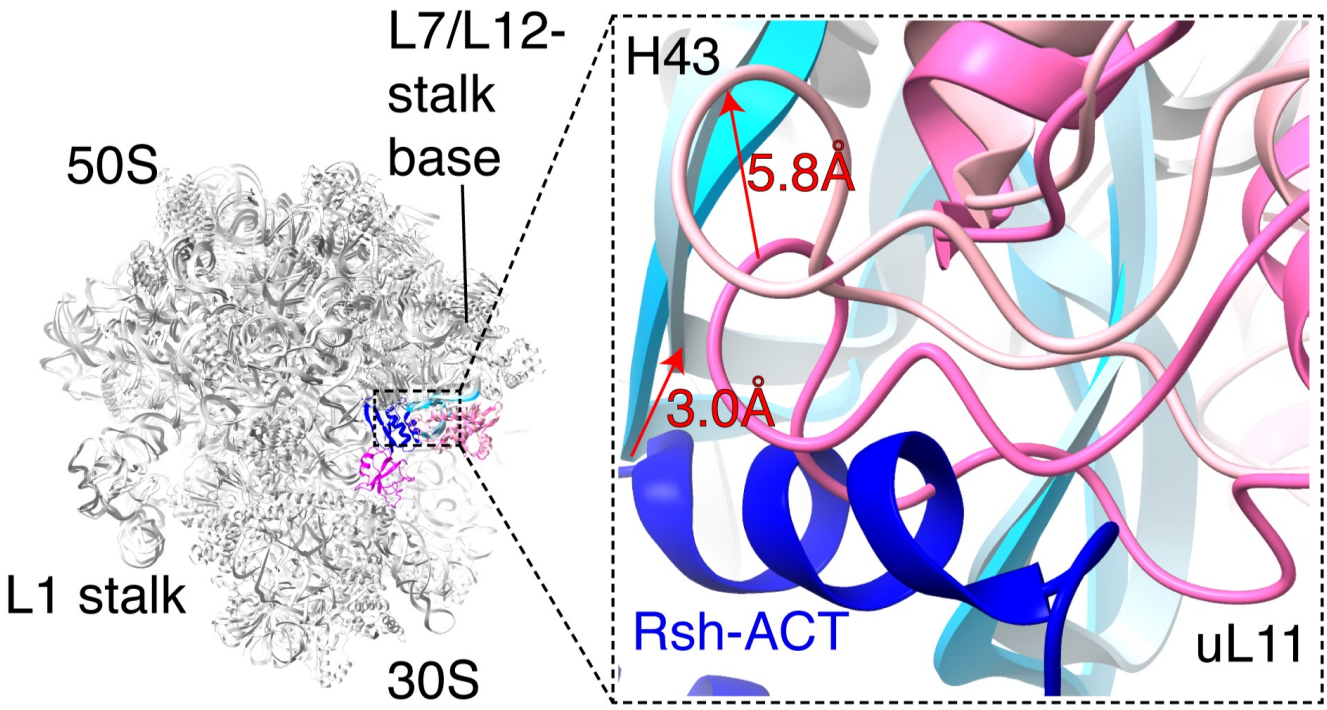

Figure S11: Rsh-binding induces rearrangement in the L7/L12-stalk base. Superimposition of the 70S-fMet-tRNA$_i^{fMet}$-Rsh (Map II) and 70S-fMet-tRNA$_i^{fMet}$ (Control) structures by aligning the 23 rRNA within their LSUs. H43 is shown in light blue and cyan. uL11 is shown in light pink and hot pink. The shifts in H43 and uL11 from control to Rsh bound state are indicated with red arrows.

Table S1: List of plasmids and strains

Plasmids	Remarks	Reference
pJl37	P_{hsp60}-based expression vector for mycobacteria; *kan*^{r}	[1]
pMH94	L5-attp-based integrative vector for mycobacteria; *kan*^{r}	[1]
pYUB854	Cosmid vector, hygr	[1]
pTTPla	Tweety-attp-based integrative vector for mycobacteria; *kan*^{r}	[1]
pLam12	$P_{acatamidase}$-based expression vector for mycobacteria; *kan*^{r}	[1]
pJV53-SacB	Sucrose-sensitive marker SacB cloned in pJV53 @ SpeI site; *kan*^{r}	[1]
pET21b	Vectors carry an N-terminal T7-Tag sequence plus an optional C-terminal His Tag sequence, *amp*^{r}	[1]
pYL3	*kan*^{r} cassette in pMH94@EcoRV & NotI sites is replaced by *hyg*^{r} cassette from pYUB854; *hyg*^{r}	[2]
pYL40	*Msmeg_6069* internal deletion in pYL42 backbone @ SacI & XbaI, *hyg*^{r}	[1]
pYL53	MSMEG_6065-6070 cloned in pYL3 @ SacI+XbaI under a constitutive promoter (P^{const}): mutant variant of $P^{zur\text{-}box}$, *hyg*^{r}	[1]
pYL155	C-terminally FLAG-tagged *mrf* with P^{zurbox} cloned in pTTPla @ SacI & XbaI sites; *kan*^{r}	[1]
pYL181	C-terminally FLAG-tagged *mrf* with P^{zurbox} cloned in pYL180 @ SacI & XbaI sites; *apr*^{r}	[1]
pYL206	L5-attp-based integrative vector carrying tet-inducible dCas9 and gRNA complementary to Clpp1; *kan*^{r}	[1]
pYL222	*Msmeg_6069* with all six his/cys mutations (H to A, C to A) and Flag tag at C-terminal and $p^{zur\text{-}box}$ cloned in plam12 @ XbaI & HindIII sites; *kan*^{r}	This Study
pYL238	*MSMEG_2965* + 500 bp UPS cloned in pMH94 @ KpnI & XbaI; *kan*^{r}	This Study
pYL240	*MSMEG_2965* with C666G mutation + 500 bp UPS cloned in pMH94 @ KpnI & XbaI; *kan*^{r}	This Study
pYL241	*MSMEG_2965 with D691R mutation* + 500 bp UPS cloned in pMH94 @ KpnI & XbaI; *kan*^{r}	This Study
pYL242	*MSMEG_2965 with C692F mutation* + 500 bp UPS cloned in pMH94 @ KpnI & XbaI; *kan*^{r}	This study
pYL243	*MSMEG_2965* with N-terminal His-tag cloned in pET21b @ NdeI & HindIII; *amp*^{r}	This study
pYL246	*MSMEG_2965* (C666G) with N-terminal His-tag cloned in pET21b @ NdeI & HindIII; *amp*^{r}	This study
pYL247	*MSMEG_2965* (D691R) with N-terminal His-tag cloned in pET21b @ NdeI & HindIII; *amp*^{r}	This study
pYL248	*MSMEG_2965* (C692F) with N-terminal His-tag cloned in pET21b @ NdeI & HindIII; *amp*^{r}	This study
pYL259	*MSMEG_2965* + 500 bp UPS cloned in pYL3 @ KpnI & XbaI; *hyg*^{r}	This study
pYL260	*MSMEG_2965* (C666G)+ 500 bp UPS cloned in pYL3 @ KpnI & XbaI; *hyg*^{r}	This study
pYL261	*MSMEG_2965* (D691R)+ 500 bp UPS cloned in pYL3 @ KpnI & XbaI; *hyg*^{r}	This study
pYL262	*MSMEG_2965* (C692F)+ 500 bp UPS cloned in pYL3 @ KpnI & XbaI; *hyg*^{r}	This study
Strains	Remarks	Reference
mc^{2}155 (WT)	High-Frequency Transformation strain of *M. smegmatis* as parent wild-type	[2]
Δmsm$_{c\text{-}}$	Unmarked Δ*Msmeg_6065-6070* in mc^{2}155	[2]
Δ*mrf (YL1)*	Unmarked Δ*c*- operon harboring pYL40; *hyg*^{r}	[1]
Δ*mrf*comp (YL2)	Unmarked Δ*c*- operon harboring pYL40 and pYL155; *hyg*^{r}, *kan*^{r}	[1]
Δ*mpy* (YL3)	Unmarked Δ*Msmeg_1878* in mc^{2}155	[2]
Δ*mpy*/Δ*mrf* (YL4)	Unmarked Δ*Msmeg_6065-6070*/Δ*Msmeg_1878* harboring pYL40; *zeo*^{r}, *hyg*^{r}	[1]
Δ*zur* (YL5)	Unmarked Δ*Msmeg_4487* in mc^{2}155	[2]
Δ*zur*/Δmrf (YL6)	Unmarked Δ*Msmeg_6065-6070* /Δ*zur* harboring pYL40; *hyg*^{r}	[1]
YL9	Δ*zur* harboring pYL181 and pYL206; *apr*^{r}, *kan*^{r}	[1]
Δ*rsh*	Δ*Msmeg_2965* in mc^{2}155, *zeo*^{r}	This Study

Table S2: List of oligonucleotides

Name	Sequence	Used in:
His1-R	GGTGCGGACGACGACAGCGCCGTCGAAGGTGGCGCTGACGAGCAGGGT	pYL222
His1-F	ACCCTGCTCGTCAGCGCCACCTTCGACGGCGCTGTCGTCGTCCGCACC	
His2-R	GGCCGAGACGGCTCCGGCCACCAGCTCAAGTAC	
His2-F	GTACTTGAGCTGGTGGCCGGAGCCGTCTCGGCC	
His3-R	CACGTCGGCGCGCCGGGCCAGACGGCGAAGCAGGAT	
His3-F	ATCCTGCTTCGCCGTCTGGCCCGGCGCGCCGACGTG	
p6069-CXXCR	ATCGTCACGCACGGTGGCCGAGACGGCTCCGTGCACCAGCTC	
p6069-CXXCF	GAGCTGGTGCACGGAGCCGTCTCGGCCACCGTGCGTGACGAT	
Pz^{urbox} 6069-XF	CGCGCCGTTCGTCTAGACGCTGCACCAGTTCTCGCC	
p6069-FLAGHR	GGCCGGAAGCTTTCACTTATCGTCGTCATCCTTGTAATCCGATTGCTCTCCTGT	
pRshMS-up500KpnIF	CTTCCCCGAACCGGTACCCCAGTTCAAGGACCTCAC	pYL236,240,241,242,256,259,260,261,262
pRshMS-XbaIFLAGR	CGAACCTCTAGATTACTTATCGTCGTCATCCTTGTAATCGGCCGCGCTGGTGACGCG	
RshC666G-F	ACCAAGCTGGCCAAGGGCTGCACCCCGGTGCCG	pYL240,246,260
RshC666G-R	CGGCACCGGGGTGCAGCCCTTGGCCAGCTTGGT	
RshD691R-F	AGCGTGCACCGCACCCGTTGCACCAACGCCGAG	pYL241,247,261
RshD691R-R	CTCGGCGTTGGTGCAACGGGTGCGGTGCACGCT	
RshC692F-F	GTGCACCGCACCGACTTCACCAACGCCGAGTCG	pYL242,248,262
RshC692F-R	CGACTCGGCGTTGGTGAAGTCGGTGCGGTGCAC	
prsh-NdeIHISF	TGACACATATGCACCACCACCACCACCACGTCGACGAGCCAGGCAAG	pYL243,246,247,248
prsh-HindIIItgaR	CGCCGAACCGCTAAGCTTTCAGGCCGCGCTGGTGACGCG	

Table S3: Data collection, Refinement and Model Validation parameters

	Map II
Data collection	
Microscope	FEI Titan Krios
Voltage (kV)	300
Pixel size (Å)	0.846
Defocus range (μm)	-1.50 to -2.50
Average e^- dose per image (e^-/ Å^2)	66.59
Particles (initial)	1,928,609
Particles (final)	36,321
FSC-threshold	0.143
Resolution (Å)	2.7
Map-sharpening B factor (Å^2) overall	-44.3
Refinement	
RMS deviations	
Bonds (Å)	0.01
Angles (^{o})	0.949
MolProbity score	1.63
Clash score	3.66
Rotamer outliers (%)	0.06
Ramachandran plot	
Outliers (%)	0.06
Allowed (%)	7.55
Favored (%)	92.39
RNA	
Correct sugar puckers (%)	99.3
Angle outliers (%)	0.00
Bond outliers (%)	0.00
Good backbone conformations (%)	78.77
Model composition	
RNA bases	4,843
Protein residues	6,299

> Sequence of codon optimized synthetic IF2:

ATACGAGAACCATatgCACCACCACCACCACCACCAGGCACCGGTCGTGGGAGGGGTAAGACTTCCTCA
CGGTAACGGCGAGACGATCCGTCTGGCACGCGGCGCTTCATTATCAGATTTTGCTGAAAAGATAAATG
CGAATCCGGCTTCACTTGTGCAGGCATTGTTCAATCTTGGAGAAATGGTTACTGCCACGCAAAGTGTCG
GTGATGAAACACTTGAGCTGTTAGGGTCGGAGATGAATTACAATGTACAGGTCGTATCACCAGAAGACG
AGGACCGTGAATTGCTTGAAAGCTTTGATTTAACCTACGGCGAAGACGCGGGTGACGAGGAGGACTTA
GAGGTGCGTCCACCCGTTGTAACCGTTATGGGCCATGTCGATCATGGTAAGACTAGACTTCTGGACAC
AATCCGGAAGGCAAATGTGAGAGAGGGCGAGGCCGGCGGTATAACGCAGCACATCGGGGCCTATCAG
GTTGAGGTTGATTTGGACGGGACGGTGCGTCCCATAACTTTTATTGATACTCCCGGTCACGAGGCCTTT
ACCGCAATGCGTGCCAGAGGTGCCAAGGCTACAGATATTGCTATTTTAGTGGTAGCCGCGGATGATGG
CGTGATGCCTCAAACGGTTGAAGCGATTAACCACGCACAGGCCGCGGACGTTCCGATAGTGGTAGCA
GTCAACAAAATTGATAAGGAAGGAGCGGACCCCGCTAAAATTCGTGGGCAGTTAACAGAATATGGATTA
ATACCGGAAGAGTATGGCGGAGACACCATGTTTGTAGATATCAGTGCGAAACAGGGAACAAATATTGAA
GCATTATTAGAAGCAGTGATTCTTACCGCAGACGCCTCTTTAGATTTGCGTGCAAACCCCGATATGGAA
GCTCAGGGAGTCGCTATAGAAGCCCATCTTGACAGAGGTCGGGGTCCTGTTGCTACTGTATTGATACA
GCGCGGCACCCTTCGGGTTGGTGATTCCGTTGTTGCGGGTGACGCTTATGGGAGAGTCCGGAGAATG
ATCGATGAACATGGAGAGGACGTCGAAGAAGCATTGCCGTCTCGGCCGGTCCAGGTAGTTGGTTTCAC
CTCGGTACCCGGCGCTGGGGACAATTTTTTAGTTGTAGATGAAGATCGGATCGCGCGTCAAATCGCGG
ATCGCCGGTCAGCGCGTAAACGGAACGCCCTTGCTGCACGTAGTCGCAAACGGATCAGCTTGGAGGA
CTTAGACTCCGCCCTTAAAGAGACGTCGCAATTAAACCTTATATTAAAAGGAGACAACGCGGGGACAGT
TGAAGCACTGGAAGAGGCCTTAATGGGAATCCAGGTGGACGACGAGGTAGAACTGCGCGTCATCGAC
CGCGGTGTCGGAGGCGTCACAGAAACGAATGTAAACTTAGCAAGTGCCTCGGACGCGATTATCATTGG
TTTTAACGTCCGGGCTGAAGGAAAGGCGACTGAATTGGCTAATAGAGAAGGAGTTGAAATACGCTATTA
TTCTGTAATCTACCAGGCGATTGATGAAATTGAAGCAGCACTTAAAGGAATGCTGAAGCCTGTATACGA
AGAGAAGGAGCTTGGGCGTGCAGAAATACGTGCCATCTTCCGCAGTTCTAAGGTGGGCAATATAGCTG
GCTGCCTTGTCACATCAGGAATAATGCGCCGCAACGCTAAGGCCCGTTTATTAAGAGACAATGTAGTAG
TTGCACAGAATTTGACGGTAAGTAGTTTAAGACGCGAAAAGGATGACGTAACGGAAGTTCGTGATGGTT
ACGAGTGCGGACTGACCTTAACCTATAATGACATCAAAGAAGGTGACGTAATTGAGACTTATGAATTAG
TTGAAAAAGCGCGTACTtgaCTCGAGTGGCCGATCC